RSC Advances

ROYAL SOCIETY OF CHEMISTRY

www.rsc.org/advances

Non-pitch coal-based activated coke introduced CeO_x and/or MnO_x for low temperature selective catalytic reduction of NO_x by NH_3

Yali Fu[a], Yongfa Zhang[a]*, Guoqiang Li[a], Jing Zhang[a], Fang Tian[b]

Abstract

Modified activated coke was prepared by introducing CeO_x and MnO_x on non-pitch coal-based activated coke (NPAC) using a novel non-pitch binder. Employing a fixed bed reactor and N_2 adsorption-desorption, X-ray diffraction, and X-ray photoelectron spectroscopy techniques, we investigated the changes of surface functional groups, pore structure characteristics, denitrification activity and adsorption behavior. It was also found that the presence of Ce^{3+} and Ce^{4+} species, promoting NO oxidation adsorption, significantly increased the starting denitrification activity and the catalysis of Mn species, helping NH_3 adsorption, showed a gradual increase in activity after a time delay. For co-impregnation modification of MnO_x and CeO_x, the manganese species and cerium species incorporated activated coke to formed Cerium Manganese Carbide. With the increase in impregnation amount, the graphite crystalline structure was destroyed, causing the degree of graphitization to be reduced and the peak of $Mn2p_{3/2}$ to be shifted to a lower binding energy. The addition of CeO_x played an important role in changing the existing state of the manganese oxide and adding MnO_x contributed to the oxidation of Ce^{3+} to Ce^{4+}. On the MnO_x-CeO_x-7.40 adsorbed NH_3 can react with adsorbed NO_x species(adsorbed NO_3 and NO_2) following Langmuir–Hinshelwood mechanism. The denitrification rate of MnO_x-CeO_x-7.40 at 140°C was as high as 75.36%.

Keywords

non-pitch; modified activated coke; MnO_x and CeO_x; low temperature; NO_x removal

1. Introduction

Currently, the control of NO_x emissions has attracted increasing attention due to its pollutants in acid rain and photochemical pollution. The selective catalytic reduction (SCR) of NO with NH_3, at a reaction temperature of 300–400°C, has proven to be the most efficient denitrification technology to date [1]. However, the catalysts in SCR technology are expensive to produce and are susceptible to poisoning by dust, SO_2, and H_2O, leading to deactivation. This necessitates the use of precipitators and desulfurization devices, which have a flue gas temperature usually below 150°C, in front of the SCR unit to prevent catalyst poisoning [2]. The development of low-temperature catalysts for the removal of NO_x at temperatures of 100–150 °C in order to avoid reheating the flue gas and thus to reduce energy consumption, is therefore an issue that is currently of great interest to researchers. The major carriers of low-temperature catalysts are TiO_2, ZSM-5, Al_2O_3 and activated carbon (coke), and the main active ingredients are CuO_x, V_2O_5, MnO_x and CeO_x, among others [3-8]. Adding cerium into Cu/ZSM-5 catalyst increases copper dispersion and mobility of lattice oxygen, and is helpful in generating higher valence copper. This improves CuCe/ZSM-5 redox properties and denitrification activity at low temperature [4]. V_2O_5 introduced into activated semi-coke or activated carbon [9-11] provides the Lewis acid sites to absorb NH_3, and promotes formation of the main intermediates of $-NH_2$ in the SCR reaction. In addition, V_2O_5 is conducive to the oxidation of NO to NO_2. It is found that the NH_3-SCR reaction mainly occurs between adsorbed NO_2 and coordinated NH_3 at low temperature. When the temperature is varied from 100°C to 150°C, the catalytic activity is poor and the denitrification rate is below 55%. In addition, the presence of cerium oxides increases the denitrification activity of the catalyst via the redox shift between Ce^{4+} and Ce^{3+} under oxidizing and reducing conditions, and the manganese oxidation states are closely related to the conversion of nitrogen oxides. For example, Mn_2O_3 and MnO_2 can improve the catalyst selectivity of NO converted into N_2 and the capacity of the NO oxidation for NO_2 [12-14]. Xin Gao[15] studied the MnO_x/3DOMC catalyst, and it shows better activity and H_2O and/or SO_2 resistance ability in low temperature. Moreover, the co-dipping of manganese or cerium and other metal oxides can also synergistically enhance catalytic performance. The catalyst SnO_2 with CeO_2/TiO_2 introduced exhibits better reaction activity arising from the increase in SCR reactive sites and decrease in the amount of adsorbed nitrate species[8] . S. Sumathi [16], however, considered that the cerium oxide was likely in a less active state at temperatures below 150°C. The capability of CeO_2 to store and release O_2 is less; hence, the denitrification rate is below 50% after 220 min of reaction. As is evident from the

[a] *Key Laboratory of Coal Science and Technology, Ministry of Education and Shanxi Province, Taiyuan University of Technology, Taiyuan030024, P.R. China. E-mail: yongfaz@yeah.net*

[b] *Department of Chemistry, Taiyuan Normal University, Taiyuan 030024, P.R. China*

preceding discussion, there are a variety of understandings for the reaction mechanisms of active ingredients such as CuO, CeO_2, V_2O_5, and Mn_2O_3. But it is uncommon to study systematic the physical and chemical properties and the adsorption behavior of NH_3 and NO on the activated coke under the low temperature 140°C in SCR reaction, which plays an important role in further enrich and improve the low temperature (100–150°C) denitrification mechanism.

Besides, for the support of activated coke(AC), the binder is an important factor influenced its property and price. The tar and pitch were used currently in the preparation of AC, which increased its cost and limited its wider application. In order to reduce production costs, a novel non-pitch binder [17, 18] was developed by our research group, which is an inexpensive and novel binder with independent intellectual property rights. The self-developed low-cost non-pitch coal-based activated coke(NPAC) was prepared by adding the non-pitch binder using the treatment of pollutants. In our previous work, they were studied that the desulfurization activity and organic matter adsorption in micro-polluted water of NPAC[19, 20]. However, the denitrification activity of NPAC needs to be improved further. In the present study, modified non-pitch coal-based activated coke was prepared by introducing CeO_x and/or MnO_x on NPAC. This work investigated the changes in surface functional groups, pore structure characteristics, denitrification activity with increasing denitrification time and adsorption behavior of NH_3 and NO in the SCR process, understood the improvement reason of denitrification activity, the role of NH_3 and NO on modified activated coke, and explored the efficient activated coke. That will be of practical importance in denitrification catalyst development in low temperature and improvement of NO_x removal.

2. Experimental

2.1 Catalyst preparation

The columnar non-pitch coal-based activated coke (NPAC) was first prepared by adding a novel low-cost clean non-pitch binder. In our previous work, we investigated the desulfurization activity and organic matter adsorption in micro-polluted water of NPAC, which have a sulfur capacity of up to 32.68 mg/g and removal rate of COD reached 83.76%[19, 20]. Other reagents used in this study, such as $Mn(CH_3COO)_2$, $Ce(NO_3)_3{\cdot}6H_2O$, were purchased from Tianjin Guangfu Fine Chemical Research Institute and Tianjin Yongda Chemical Reagent Development Center as analytically pure (AR) reagents.

The NPAC was first crushed and sieved into 10–18 mesh particles. The process of co-precipitation for manganese oxide and/or cerium oxide on the NPAC was as follows: NPAC was first dipped into the solution containing manganese acetate ($Mn(CH_3COO)_2$) and/or cerium nitrate($Ce(NO_3)_3{\cdot}6H_2O$) at room temperature for 12 h, followed by drying in an oven at 100°C for 5 h, then calcined in oxygen-depleted atmosphere (1.5%O_2+98.5%N_2) at 500°C for 2.5h. The modified activated coke was obtained in various concentrations of $Mn(CH_3COO)_2$ and/or $Ce(NO_3)_3{\cdot}6H_2O$. In this work, three kinds of modified activated cokes were preapared: MnO_x-NPAC (Added manganese acetate), CeO_x-NPAC (Added cerium nitrate) and MnO_x-CeO_x-NPAC (Added manganese acetate and cerium nitrate). The samples were prepared using a mass fraction ratio for Mn and Ce of 0.7:1 and were denoted as MnO_x-a, CeO_x-b and MnO_x-CeO_x-b, where a and b represent the mass fractions of Mn and Ce, respectively.

2.2 Experiment

The denitrification performance tests for the prepared catalysts were conducted in a conventional fixed bed quartz reactor with a 15 mm i.d. at 140°C. For the denitrification experiments, 15.5 g of modified activated coke was loaded into the reactor. The total gas flow rate was 1600 L/min. Four feed gases (NO/N_2, NH_3/N_2, O_2, and N_2), each controlled separately by mass flow controllers, were blended in a mixing device prior to being introduced into the reactor. The experimental conditions for denitrification were as follows: 400 ppm NO, 400 ppm NH_3, 7.2 vol. % O_2, and balance N_2. Moreover, the concentrations of NO_x in the inlet and outlet gases were analyzed using a combustion gas analyzer (OPTIMA 7, MRU GmbH Germany).

The reaction results are described in terms of denitrification rate, which were calculated according to formulae (1).

$$\eta = (C_0 - C)/C_0 \times 100\%, \quad (1)$$

where η is the denitrification rate (%), C_0 is the inlet NO_x concentration (NO_x is the sum of the NO and NO_2 concentrations in ppm) and C is the outlet NO_x concentration (ppm).

Transient response experiment of NH_3 and NO were also conducted in above-mentioned quartz reactor at 140°C. In the reaction, when the denitrification rate and outlet NO_x concentration were in steady, the reaction was called into steady-state. Transient response experiment of NH_3 was as follows. After the denitrification reaction of 4 h on the modified activated coke, the denitrification rate and NO_x outlet

concentration were steady, denoted as the steady-state 1. And then stopped gases NH_3 supply, the new steady-state 2 was reached. Next, the gases NH_3 were provided again until the experiment ended. The difference between the transient response experiment of NO and that of NH_3 is stopped NO supply. In the transient response experiment, the other gases component concentration except NH_3 and NO and the total volume were constant by changing the flow of N_2, when closed or opened the gases NH_3 and NO.

2.3 Catalyst characterization

The physical characteristics of the activated coke were measured by N_2 adsorption at 77 K using an ASAP 2020 automated adsorption apparatus (Micromeritics). The sample surface area was determined by the Brunaue-Emmett-Teller (BET) equation and the total volume (V) was obtained by converting nitrogen adsorption value into liquid nitrogen volume. The micropore volume was determined from the Dubinin-Astakhov (D-A) equation and average pore size d = 4V/BET. The microporosity was the percentage of micropore volume in the total pore volume. The pore size distribution was measured by N_2 adsorption method and Mercury intrusion porosimetry (DC-PS-T110-t60) with pressure range 0~200 MPa.

X-ray diffraction (XRD) of the activated coke was performed using a Rigaku D/max-3B system with Cu Ka radiation. The catalysts were scanned at a rate of 8°/min over the range from 5° to 85°.

The surface chemical compositions of activated carbon were determined by X-ray photoelectron spectroscopy (XPS) using the Kratos Axis Ultra DLD multifunctional electron spectrometer.

The in situ diffuse reflectance infrared Fourier transform spectroscopy (DRIFTS) experiments were performed on a Nicolet 6700 FTIR spectrometer with in situ diffuse reflectance pool and high-sensitivity MTC detector. Prior to each experiment, the samples were purged in a flow of 50 mL/min N_2 at 250 °C for 0.5 h and then cooled down to 140 °C under N_2 atmosphere. The background spectrum was recorded and subtracted from the sample spectrum.

3. Results and discussion

3.1 Pore structure and BET analysis

Nitrogen adsorption isotherms at 77 K of NPAC and modified activated cokes are presented in Fig. 1. Obviously, the quantity adsorbed of modified activated cokes decreased markedly, which was attributed to the MnO_x and CeO_x particles covering the surface and blocking the pores [13, 21]. The adsorption-desorption isotherms of MnO_x-CeO_x-b appear as a hysteresis loop when relative pressure $P/P_0 > 0.4$. The quantity adsorbed increased sharply in the high relatively pressure region, which was caused by multilayer adsorption in mesopores or macropores. This indicated that the modified activated coke MnO_x-CeO_x-b contained micropores, mesopores, and macropores.

The pore structure characteristics of activated cokes are given in Table 1. The BET and micropore volume of NPAC were 261.5 $m^2 \cdot g^{-1}$and 0.1094 $cm^3 \cdot g^{-1}$, respectively, which were greater than that of modified activated coke. For MnO_x-1.31 and CeO_x-439, total volume, microporosity and average pore size have little change. However, for MnO_x-CeO_x-b, total volume enlarged from 0.1098 $cm^3 \cdot g^{-1}$ to 0.2840 $cm^3 \cdot g^{-1}$, microporosity decreased significantly from 57.38% to 18.27%, and average pore size increased from 3.460 nm to 10.51 nm. These suggested that pore structure was changed in the process of modification, resulting in enlarged pore size, reduction in micropores, and an increase in mesopores and/or macropores.

Table 1 Pore structure properties of activated coke.

Sample	BET ($m^2 \cdot g^{-1}$)	Total volume ($cm^3 \cdot g^{-1}$)	Micropore volume($cm^3 \cdot g^{-1}$)	Microporosity (%)	Average pore size(nm)
NPAC	261.5	0.1399	0.1094	78.20	2.140
MnO_x-1.31	135.3	0.1026	0.07310	71.25	3.030
CeO_x-4.39	126.3	0.0913	0.06980	76.45	2.890
MnO_x-CeO_x-0.50	127.1	0.1098	0.06300	57.38	3.460
MnO_x-CeO_x-2.60	96.49	0.2441	0.04550	18.64	10.12
MnO_x-CeO_x-4.39	108.1	0.2840	0.05190	18.27	10.51
MnO_x-CeO_x-7.40	122.0	0.2804	0.05840	20.83	9.190

N_2 adsorption method has some limitations, when the quantity adsorbed increased sharply in the high relatively pressure region(Fig. 1) or there were some macropores. But, the mercury intrusion porosimetry can make up the defects of N_2 adsorption method. So, the pore size distribution of MnO_x-CeO_x-b measured by N_2 adsorption method and Mercury intrusion porosimetry is showed in Table 2. For mercury intrusion porosimetry, with increase of MnO_x and CeO_x impregnation content, the average pore size had little change, the pore volume of

mesopores range from 7 to 50nm reduced, and the pore volume of macropores(>50nm) increased gradually. It can be obtained that the pore volume of mesopore (2~50nm) by adding pore Volume of 2~7nm and that of 7~50nm. For MnO_x-CeO_x-0.5, MnO_x-CeO_x-2.60, MnO_x-CeO_x-4.39 and MnO_x-CeO_x-7.40, the corresponding mesopore volume was 0.4861, 0.3962, 0.3657 and 0.2046 ml/g, respectively. These suggests that the mesopores developed into macropores or collapsed in the process of modification. Combination with the advantages of two test methods, the average pore sizes of MnO_x-CeO_x-2.60, MnO_x-CeO_x-4.39 and MnO_x-CeO_x-7.40 are more reliable by Mercury intrusion porosimetry.

Table 2 Pore size distribution by N_2 adsorption method and Mercury intrusion porosimetry

Sample	N_2 adsorption method			Mercury intrusion porosimetry		
	Pore Volume(ml/g)		Average pore size(nm)	Average pore size(nm)	Pore Volume(ml/g)	
	<2nm	2~7nm			7~50nm	>50nm
MnOx-CeOx-0.50	0.06300	0.02110	3.460	8.055	0.4650	0.001000
MnOx-CeOx-2.60	0.04550	0.02420	10.12	8.024	0.3720	0.01400
MnOx-CeOx-4.39	0.05190	0.02370	10.51	8.070	0.3420	0.03900
MnOx-CeOx-7.40	0.05840	0.02960	9.190	8.019	0.1750	0.08900

3.2 XRD and TEM ananlysis

The XRD patterns of the catalysts are shown in Fig. 2. All samples show two broad diffraction peaks of graphite crystallite structure which can be assigned to the (002), (100) and (101) reflections, respectively. For MnO_x-1.31 (Fig. 2(A)), the characteristic peaks corresponding to (311), (222), (400) and (440) of Mn_3O_4 (JCPDs No.13-0162) were detected, indicating the presence of Mn_3O_4 phase in the catalyst. Additionally, for CeO_x-439 (Fig. 2(A)), the diffraction peaks of graphite crystallite structure become weaker and the characteristic peaks corresponding to (111), (200), (220) and (311) of CeO_2 (JCPDs No.34-0394) can be observed. These imply that the process of introducing cerium oxide into NPAC destroyed the graphite structure of NPAC, so that some structural defects appeared on the surface of catalyst CeO_x-439. As shown in Fig. 2(B), with an increase in impregnation amount, the diffraction peaks corresponding to (002) of graphite crystallite structure decreased in intensity and moved to the right, and the Bragg peaks corresponding to (100) and (101) gradually divided into two small 'left and right' peaks. This suggests that the graphite crystalline structure was destroyed in the process of modification, causing the degree of graphitization to be reduced. The diffraction peaks corresponding to (201), (120), (300) and (302) of Cerium Manganese Carbide (JCPDs No.51-1258) in the catalyst MnO_x-CeO_x-0.50 can be detected, suggesting that the manganese species and cerium species incorporated activated coke. Except for the diffraction peaks of graphite crystallite structure, the catalyst of MnO_x-CeO_x-2.60 has no clear characteristic peaks, indicating that the manganese and cerium species may exist in an amorphous or highly dispersed phase. The XRD peaks of Mn_3O_4 and CeO_2 over the catalysts MnO_x-CeO_x-4.39 and MnO_x-CeO_x-7.40 are also present, representing manganese species and cerium species being susceptible to aggregation into small crystals when the dipping amount of CeO_x is higher than 4.39%.

Fig.3 showed the TEM imaging patterns of the modified activated cokes MnO_x-1.31, CeO_x-4.39 and MnO_x-CeO_x-7.40. It can be seen that the metal oxides particles were poor dispersion on the MnO_x-1.31, CeO_x-4.39. However, a relatively homogeneous dispersion of MnO_x-CeO_x-7.40 was obtained than the sample CeO_x-4.39. The image of catalysts reveals that the metal oxides added to the NPAC located at the surface of the support and the cerium species and manganese species might promote the dispersion of each other. The fine particles over MnO_x-CeO_x-7.40 are relatively spherical in shape. The particles are obvious aggregation on the MnO_x-1.31 and CeO_x-4.39. This is agreement with those of XRD.

3.3 X-ray photoelectron spectroscopy analysis

The surface components and chemical state of the elements in the modified activated coke can be identified using XPS. XPS spectra of Mn 2p and Ce 3d are shown in Fig. 4. As seen in Fig. 4(A), the peak at around 643.4eV arising from Mn $2p_{3/2}$ of MnO_x-1.31is higher than the other peaks, which is due to the incomplete decomposition of the manganate at 644.2 ± 0.4 eV formed in the process of preparation [22]. It can also be seen that the binding energy of Mn $2p_{3/2}$ state for MnO_x-CeO_x-b was reduced from 642.5 eV to 642.0 eV, thus indicating that the peak of $Mn2p_{3/2}$ shifts to lower binding energy with increasing MnO_x and CeO_x content. According to previous literature [23, 24], these values of Mn $2p_{3/2}$ were higher than the binding energy of Mn^{2+}(640.9eV), but were intermediate between those of Mn^{3+} (641.8 eV) and Mn^{4+} (642.5 eV), suggesting the presence of Mn^{3+} and Mn^{4+} on the modified activated coke. Combining these results with the XRD analysis (Fig. 2) suggests that manganese species either aggregated into small Mn_3O_4 crystals (for MnO_x-1.31, MnO_x-CeO_x-4.39 and MnO_x-CeO_x-7.40), existed in an amorphous or highly dispersed phase (on the catalyst MnO_x-CeO_x-2.60), or incorporated activated coke (in MnO_x-CeO_x-0.50).

Fig. 4(B-F) show the Ce 3d XPS spectra of modified activated coke. Deconvolution of the Ce 3d spectra reveals the coexistence of Ce^{4+} and

Ce^{3+} species on the surface of the modified activated coke. Ce^{4+} species can be fitted into six peaks: v_0 (BE≈882.5 eV), v_1 (BE≈888.8 eV), v_2 (BE≈898.3 eV), v_0' (BE≈901.1 eV), v_1'(BE≈907.5 eV), v_2'(BE≈916.6 eV), and Ce^{3+} species can be fitted into four peaks: u_0 (BE≈884.9 eV), u_1 (BE≈880.5 eV), u_0' (BE≈903.5 eV), and u_1'(BE≈899.0 eV) [25, 26]. Using the area of representative peaks method, the relative content of Ce^{4+} and Ce^{3+} species is listed in Table 3. The ratio of Ce^{4+} to Ce^{3+} (denoted as Ce^{4+}/Ce^{3+}) for the relative content was used to represent the overall oxidation state of the cerium oxide. For MnO_x-CeO_x-4.39, the Ce^{4+} to Ce^{3+} ratio, 5.74, is higher than that of CeO_x-4.39, which is 2.50. This suggests that the addition of manganese oxide helped the transfer of electrons from Ce^{3+} to oxygen or manganese species when a solid solution was formed during the calcination process [27], thus promoting the transformation of Ce^{3+} to Ce^{4+}. For MnO_x-CeO_x-b, the ratio of Ce^{4+} to Ce^{3+} increased from 0.65 to 5.57 and then slightly decreased, indicating that the impregnation contents in a certain range contributed to oxidation of Ce^{3+} to Ce^{4+}.

Table 3 The relative content of Ce^{4+} and Ce^{3+} measured by XPS.

Sample	CeO_x-4.39	MnO_x-CeO_x-0.50	MnO_x-CeO_x-2.60	MnO_x-CeO_x-4.39	MnO_x-CeO_x-7.40
Ce^{3+}	28.53	60.45	34.43	14.83	15.21
Ce^{4+}	71.47	39.55	65.57	85.17	84.79
Ce^{4+}/Ce^{3+}	2.500	0.6500	1.900	5.740	5.570

The O1s peaks are divided into three kinds of species, which are assigned to the lattice oxygen species at 529.5~530.1eV (denoted as O_α), the chemisorbed oxygen species or/and weakly bonded oxygen species at 531.0~531.7eV (denoted as O_β), and C–O combined oxygen species at 532.7~533.5eV (denoted as Oγ) [14, 28]. The area of the peaks was used to describe the relative content of each oxygen species, as listed in Table 4. The O_α and O_β content of NPAC (0.800% and 5.070%, respectively) is lower than that of modified activated coke catalysts. The O_α and O_β content of modified activated coke MnO_x-CeO_x-7.40 increased by 33.98 times and 10.09 times, respectively, to values of 27.98% and 56.22%.The increase in O_α content could be attributed to oxygen atoms bound in the cerium oxide [29], whereas the increase in O_β content is due to structural defects appeared in the process of calcinations owing to the destruction of the graphite structure of the NPAC surface. These results are consistent with the XRD analysis described earlier. In addition, cerium species produce charge imbalances, vacancies and unsaturated chemical bonds on the surface of modified activated coke, and help to form chemisorbed oxygen species [27].

Table 4 The contents of oxygen on NPAC and modified activated coke measured by XPS.

Sample	NPAC	MnO_x-1.31	CeO_x-4.39	MnO_x-CeO_x-0.50	MnO_x-CeO_x-2.60	MnO_x-CeO_x-4.39	MnO_x-CeO_x-7.40
O_α	0.8000	0.2600	9.460	4.880	7.190	10.84	27.98
O_β	5.070	25.10	29.00	19.28	27.61	31.93	56.22
O_γ	94.13	74.64	61.54	75.84	65.20	57.23	15.79

3.4 Denitrification performance test

The denitrification activity of the activated coke, expressed as the denitrification rate, is shown in Fig. 5. Fig. 5(A) illustrates that the denitrification performance of single modified activated coke dipping CeO_x or MnO_x was superior to the NPAC. The denitrification rates of modified activated cokes CeO_x-4.39 and MnO_x-1.31 tended to become stable after a reaction time of 120 min and were 31.94% and 37.69%, respectively. This implied that the additional amount of CeO_x or MnO_x within a certain concentration range had a similar effect on the denitrification activity. Combined with the XRD (Fig. 2) and the XPS (Fig. 4) analysis, the chemisorbed oxygen content for CeO_x-4.39 increased from 5.07% to 29.00% and the Ce^{3+} and Ce^{4+} species were formed by introducing cerium oxide CeO_x into NPAC. For MnO_x-1.31, manganese oxide exited in different oxidation state or aggregated into Mn_3O_4 crystals, and the chemisorbed oxygen content increased from 5.07% to 25.10%. It is commonly acknowledged that the chemisorbed oxygen species are more active than the lattice oxygen species, and play a major role in oxidation reactions due to their higher mobility [26, 30]. After modification of NPAC, the increase of chemisorbed oxygen content improved oxidation of NO to NO_2, which caused the denitrification activity to further increase. In addition, the denitrification rate of CeO_x-4.39 declined from 75.00% to 40.27% in 30 min, while in the case of MnO_x-1.31, the starting denitrification rate was similar to that of NPAC, and then before slowly stabilizing with time after following a downward trend. This indicates that the presence of Ce^{3+} and Ce^{4+} species significantly improved the starting denitrification activity, whereas the presence of Mn species prompted a gradual increase in activity. The mechanism of manganese oxide action in the SCR reaction has been reported to be related to the adsorption of NH_3 on Lewis acid Mn^{3+} sites, which can subsequently be transformed to NH_2 in the presence of O_2 and NO [31].

As seen in Fig. 5(B), the denitrification activity of modified activated coke increased with increasing of MnO_x and CeO_x impregnation

content, elevating its denitrification rate from 27.35% to 75.36% at 220 min. From XRD and XPS analysis, it was found that the change in MnO_x and CeO_x content had a big effect on the surface functional groups in the modification process. Specifically: the manganese and cerium species co-existed in different oxidation states, the lattice oxygen and chemisorbed oxygen contents improved, and the ratio of Ce^{4+} to Ce^{3+} on the catalyst increased. The introduction of cerium species can create charge imbalances and vacancies on the catalyst surface, and increase the mobility of oxygen, resulting in an improvement of NO_x absorption and oxidation and transferability of oxygen on the activated coke surface. Several studies attributed absorption ability improvement to redox cycle between Ce^{4+} and Ce^{3+}, provide adsorbed oxygen atoms to generate C(O) sites[32]. In addition, the Ce^{4+} and Mn^{3+} species assist in both H-abstraction of NH_3 and the formation of nitrites [14, 31]. Fig. 5(B) also showed that the denitrification rate rose with time after the initial fall, and that the magnitude of change increased with an increase in the impregnated amount. For MnO_x-CeO_x-7.40, the denitrification rate decreased rapidly from 98.83% to 61.19% within 45 min, and then gradually increased to 75.36%. This is the result of interaction between the MnO_x and the CeO_x. On one hand, the existence of Ce^{4+} and Ce^{3+} on the modified activated coke surface significantly improved the oxidation of NO to NO_2, enhancing NO_2 adsorption in the start-up phase. On the other hand, the presence of Mn species in different oxidation states, especially the reduction and oxidation between Mn^{4+} and Mn^{3+}, caused the denitrification rate of modified activated coke to gradually increase. The MnO_x and CeO_x species jointly enhanced the denitrification activity of activated coke. It is also found that Mn species may be associated with NH_3 adsorption, which is decisive step to the formation of the intermediate species.

3.5 Transient response experiment

In order to further know adsorption behavior of NH_3 and NO on the modified activated cokes, the reaction process of the modified activated cokes MnO_x-1.31, CeO_x-4.39 and MnO_x-CeO_x-7.40 were studied by transient response experiment. The transient response experiment of NH_3 and NO was illustrated in Fig. 6. The Fig. 6(A-C) shows that after stopping NH_3 supply, the denitrification rate did not immediately plunge, but decreased slowly to a new steady state. This is explained by the fact that the adsorbed NH_3 reacted with NO_x, and a certain amount of NO_x was adsorbed on the surface of the modified activated coke. Under the condition of stopping NH_3 supply, the denitrification rate of MnO_x-1.31, CeO_x-4.39 and MnO_x-CeO_x-7.40 in new steady-state were 5.34%, 11.01% and 14.39%, respectively. This suggests the adsorption ability of NO_x on the MnO_x-CeO_x-7.40 is the strongest, CeO_x-4.39 is next, and MnO_x-1.31 is the weakest. That means that co-impregnation of MnO_x and CeO_x is more advantageous to NO_x adsorption. Associated with Fig. 5(A), it is found that the cause of denitrification activity for CeO_x-4.39 improved in the start-up phase is the enhancement of NO_x adsorption ability. After the gases NH_3 was provided again, the denitrification rate of the modified activated coke rose gradually, which is because the NH_3 in gaseous form was not involved in the SCR reaction. The denitrification rate of MnO_x-1.31 was a bit higher than that of the CeO_x-4.39 before stopping the NH_3 supply (Fig. 6(A-B)), but, after offering the NH_3 again, the CeO_x-4.39 took more time to reach a new steady denitrification rate than the MnO_x-1.31. Because NH_3 adsorption is the rate-limiting step in the SCR reaction[33], the adsorption of NH_3 on the MnO_x-1.31 is better than that on the CeO_x-4.39. Likewise, the denitrification rate of MnO_x-CeO_x-7.40 was much higher than that of the CeO_x-4.39, however, they took the similar time to reach the steady state. These results indicated the adsorption of NH_3 on the MnO_x-1.31 and MnO_x-CeO_x-7.40 is better than that on the CeO_x-4.39. The gradual increase of denitrification rate on the MnO_x-1.31 and MnO_x-CeO_x-7.40 (Fig. 5) was attributed to Mn species in oxidation state to improve the adsorption ability of NH_3. As showed in Fig. 6(D-F), when the gases NO was shutoff, NO_x outlet concentration decreased rapidly to below 10 ppm. When the gases NO were provided, NO_x outlet concentration of the modified activated cokes MnO_x-1.31, CeO_x-4.39 and MnO_x-CeO_x-7.40 returned quickly to the original level within 10 min, 20 min and 30 min, respectively. For the MnO_x-1.3 and CeO_x-4.39, this may be because adsorbed NH_3 species can react with the gaseous NO in SCR reaction following Eley-Rideal mechanism or because NO species are easy to translate into adsorbed NO species, which can react with adsorbed NH_3 species following Langmuir–Hinshelwood mechanism. For the MnO_x-CeO_x-7.40, adsorbed NH_3 species can react with adsorbed NO species (Langmuir–Hinshelwood mechanism).

3.6 DRIFTS

In order to find out the adsorbed NH_3 species and NO species on the modified activated cokes, the in situ DRIFTS of NH_3+O_2 adsorption and NO+O_2 adsorption were studied. The catalyst was first heated at 250°C for 0.5h in flow of N_2 and then cooled down to 140°C. At this temperature, the flow switched to 800ppmNH_3/N_2+7.2%O_2/N_2 to adsorb NH_3 for 20min or the flow witched to 800ppmNO/N_2+7.2%O_2/N_2 to adsorb NO followed by N_2 purging. DRIFTS spectra(Fig. 7) of NH_3 adsorbed on the MnO_x-1.31 showed strong bands at 1298, 1361, 1479 and 1512 cm^{-1} and weak bands at 1177, 1697cm^{-1}. Those bands of the CeO_x-4.39 and MnO_x-CeO_x-7.40 were very weak, suggesting more NH_3

adsorbed on the MnO_x-1.31. This is consistent with the analysis of the transient response experiment. The band at 1177 and 1298 cm^{-1} was attributed to the symmetric deformation vibration of NH_3 coordinatively to one type of lewis acid site[9]. The band at 1361 cm^{-1} could be assigned to the intermediate from oxidation of NH_3[34] and the bands at 1512 cm^{-1} belonged to some amide species such as -NH_2. The bands at 1479 and 1697 cm^{-1} could be due to the NH^{4+} species. For MnO_x-1.31 and MnO_x-CeO_x-7.40, there were a big negative bands at 1065cm^{-1} attributed to coordinated NH_3 at Mn^{3+} sites. The above analysis indicated that lewis acid sites or manganese species promoted NH_3 adsorption and cerium species had no obvious effect of that. The negative bands at 883, 1408 and 1631cm^{-1} were ascribed to the transformation and vanish of =C-H, -COO- and C=O groups on the support surface. These results revealed that absorbed NH_3 species on the surface of MnO_x-CeO_x-7.40 were mainly coordinated NH_3 and oxides species, those of MnO_x-1.31 were coordinated NH_3, oxides species, amide species and NH^{4+} species, and those of CeO_x-4.39 were amide species and NH^{4+} species.

Fig. 8 shows DRIFTS spectra of NO + O_2 adsorbed on CeO_x-4.39, MnO_x-1.31 and MnO_x-CeO_x-7.40. As can be seen, the strong adsorption bands at 1375 cm^{-1} and the bands at 801, 1598, 1630, 1678, 1849 and 1906 cm^{-1} were detected. The strong bands at 1375 cm^{-1} are assigned to absorbed NO_3 which is produced by the disproportionation of chemisorbed NO_2 on the catalyst surface[35]. The band of MnO_x-CeO_x-7.40 attributed to absorbed NO_3 was strongest, that of CeO_x-4.39 was next, and that of MnO_x-1.31 was weakest. This suggested that the cerium species are more beneficial to the oxidation and adsorption of NO_x than those of the Mn species. The bands at 1598, 1630 cm^{-1} are observed due to absorbed NO_2 and the weak bands at 1849 and 1906 cm^{-1} are attributed to absorbed NO. Another the bands are detected at 801 and 1678 cm^{-1} due to the stretching vibration of O-N and O-N=O. The negative bands at 1072 and 2981cm^{-1} were ascribed to the transformation and vanish of C-O groups and aliphatic species on the support surface, respectively. The negative bands due to C-O groups and aliphatic species of CeO_x-4.39 and MnO_x-CeO_x-7.40 are stronger than MnO_x-1.31, which is most likely from the oxidation function of cerium species. These revealed that absorbed NO species on the modified activated cokes surface are mainly absorbed NO_3 and absorbed NO_2, and NO adsorption is weak.

Recently, the fast SCR progress (Equation 1) has been developed that has faster reaction rate (almost 10 times) and high NO_x removal efficiency than the standard SCR (Equation 2)[28, 36]. These results of implied that the one main reason of enhancing denitrification activity may be the oxidation of NO, which caused the formation of absorbed NO_2 and absorbed NO_3. Besides, the other reason is the increase of absorbed NH_3 species.

$$4NH_3 + 2NO + 2NO_2 \rightarrow 4N_2 + 6H_2O \quad \text{(Eq. 1)}$$

$$4NH_3 + 4NO + O_2 \rightarrow 4N_2 + 6H_2O \quad \text{(Eq. 2)}$$

4. Conclusions

The high activity and low cost modified activated coke MnO_x-CeO_x-7.40 were prepared by MnO_x and CeO_x co-impregnation. The denitrification rate of sample MnO_x-CeO_x-7.40 at 140°C was as high as 75.36%.

After single modification of CeO_x or MnO_x, the denitrification performance of modified activated coke was superior to the NPAC. It was also found that the presence of Ce^{3+} and Ce^{4+} species, promoting NO adsorption by absorbed NO_2 and absorbed NO_3, significantly increased the starting denitrification activity as compared to the catalysis of Mn species, improving NH_3 adsorption by the formation of coordinated NH_3, amide species, oxides species and NH^{4+} species, which showed a gradual increase in activity after a time delay. For the modification of MnO_x and CeO_x by co-impregnation, the addition of CeO_x played an important role in changing the existing state of the manganese oxide, and the dipping amount in a certain range contributed to oxidation of Ce^{3+} to Ce^{4+} on the activated coke surface. Besides, the manganese species and cerium species incorporated activated coke to formed Cerium Manganese Carbide. With the increase in impregnation amount, the graphite crystalline structure was destroyed. This caused the degree of graphitization to be reduced, the $Mn2p_{3/2}$ peak to be shifted to a lower binding energy, and the amount of chemisorbed oxygen species and the ratio of Ce^{4+} to Ce^{3+} to be increased. Thus, we have demonstrated in this work that the existence of manganese and cerium species in different oxidation states could jointly enhanced NH_3 species adsorption and NO_x species oxidation to improve the denitrification activity of modified activated coke. On the MnO_x-CeO_x-7.40 surface, adsorbed NH_3 species can react with adsorbed NO species (adsorbed NO_3 and NO_2) following Langmuir–Hinshelwood mechanism.

Acknowledgements

This project is supported by the Natural Science Foundation of China (No. 51274147).

Reference

1. L. Chen, J. Li and M. Ge, *The Journal of Physical Chemistry C*, 2009, **113**, 21177-21184.
2. J. Liu, Z. Huang, Z. Li, Q. Guo and Q. Li, *Chemical Journal of chinese universities*, 2014, **35**, 589-595.
3. Y.-F. Qu, J.-X. Guo, Y.-H. Chu, M.-C. Sun and H.-Q. Yin, *Applied Surface Science*, 2013, **282**, 425-431.
4. B. Dou, G. Lv, C. Wang, Q. Hao and K. Hui, *Chemical Engineering Journal*, 2015, **270**, 549-556.
5. Y. Peng, J. Li, X. Huang, X. Li, W. Su, X. Sun, D. Wang and J. Hao, *Environmental science & technology*, 2014, **48**, 4515-4520.
6. J. Amanpour, D. Salari, A. Niaei, S. M. Mousavi and P. N. Panahi, *Journal of environmental science and health. Part A, Toxic/hazardous substances & environmental engineering*, 2013, **48**, 879-886.
7. J. R. D. Iorio, S. A. Bates, A. A. Verma, W. N. Delgass, F. H. Ribeiro, J. T. Miller and R. Gounder, *Topics in Catalysis*, 2015, **58**, 1-11.
8. L. Zhang, L. Li, Y. Cao, Y. Xiong, S. Wu, J. Sun, C. Tang, F. Gao and L. Dong, *Catal.sci.technol*, 2015, **5**, 2188-2196.
9. J. Wang, Z. Yan, L. Liu, Y. Chen, Z. Zhang and X. Wang, *Applied Surface Science*, 2014, **313**, 660-669.
10. Z. Lei, B. Han, K. Yang and B. Chen, *Chemical Engineering Journal*, 2013, **215**, 651-657.
11. D. Sun, Q. Liu, Z. Liu, G. Gui and Z. Huang, *Catalysis letters*, 2009, **132**, 122-126.
12. F. Cao, J. Xiang, S. Su, P. Wang, L. Sun, S. Hu and S. Lei, *Chemical Engineering Journal*, 2014, **243**, 347-354.
13. M. Wang, H. Liu, Z.-H. Huang and F. Kang, *Chemical Engineering Journal*, 2014, **256**, 101-106.
14. L. Qu, C. Li, G. Zeng, M. Zhang, M. Fu, J. Ma, F. Zhan and D. Luo, *Chemical Engineering Journal*, 2014, **242**, 76-85.
15. X. Gao, L. Li, L. Song, T. Lu, J. Zhao and Z. Liu, *RSC Advances*, 2015, **5**, 29577-29588.
16. S. Sumathi, S. Bhatia, K. T. Lee and A. R. Mohamed, *Chemical Engineering Journal*, 2010, **162**, 51-57.
17. *China Pat.,* CN103113949A, 2013.
18. D. Dong, Y. Zhang, Y. Zhao and Q. Wang, *Chemistry Letters*, 2014, **43**, 1470-1472.
19. J. L. Ding, Thesis, Taiyuan University of Technology, 2013.
20. J. L. Ding, Y. Q. Zhao, Y. F. Zhang and Y. L. Fu, *Applied Mechanics and Materials*, 2013, **316-317**, 1055-1058.
21. S. M. Lee, K. H. Park and S. C. Hong, *Chemical Engineering Journal*, 2012, **195-196**, 323-331.
22. D. A. Pena, B. S. Uphade and P. G. Smirniotis, *Journal of catalysis*, 2004, **221**, 421-431.
23. E. López-Navarrete, A. Caballero, A. R. González-Elipe and M. Ocaña, *Journal of the European Ceramic Society*, 2004, **24**, 3057-3062.
24. V. Di Castro and G. Polzonetti, *Journal of Electron Spectroscopy and Related Phenomena*, 1989, **48**, 117-123.
25. F. Larachi, J. Pierre, A. Adnot and A. Bernis, *Applied Surface Science*, 2002, **195**, 236-250.
26. D. Zhang, L. Zhang, C. Fang, R. Gao, Y. Qian, L. Shi and J. Zhang, *RSC Advances*, 2013, **3**, 8811.
27. Z. Wu, R. Jin, Y. Liu and H. Wang, *Catalysis Communications*, 2008, **9**, 2217-2220.
28. Y. Wang, C. Ge, L. Zhan, C. Li, W. Qiao and L. Ling, *Industrial & Engineering Chemistry Research*, 2012, **51**, 11667-11673.
29. J. Beran, S. Hishita, K. Mašek, V. Matolín and H. Haneda, *Ceramics International*, 2014, **40**, 323-329.
30. K. Li, X. Tang, H. Yi, P. Ning, D. Kang and C. Wang, *Chemical Engineering Journal*, 2012, **192**, 99-104.
31. W. S. Kijlstra, D. S. Brands, H. I. Smit, E. K. Poels and A. Bliek, *Journal of Catalysis*, 1997, **171**, 219-230.
32. F. Cao, J. Chen, M. Ni, H. Song, G. Xiao, W. Wu, X. Gao and K. Cen, *RSC Advances*, 2014, **4**, 16281-16289.
33. Z. Zhu, Z. Liu, S. Liu and H. Niu, *Fuel*, 2000, **79**, 651-658.
34. G. Qi and R. T. Yang, *The Journal of Physical Chemistry B*, 2004, **108**, 15738-15747.
35. J. A. Rodriguez, T. Jirsak, G. Liu, J. Hrbek, J. Dvorak and A. Maiti, *Journal of the American Chemical Society*, 2001, **123**, 9597-9605.
36. M. F. Irfan, J. H. Goo and S. D. Kim, *Applied catalysis B: environmental*, 2008, **78**, 267-274.

Figures

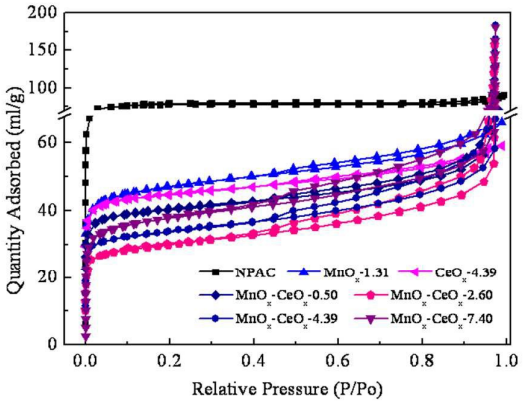

Fig. 1 N_2 adsorption–desorption isotherms obtained at 77 K.

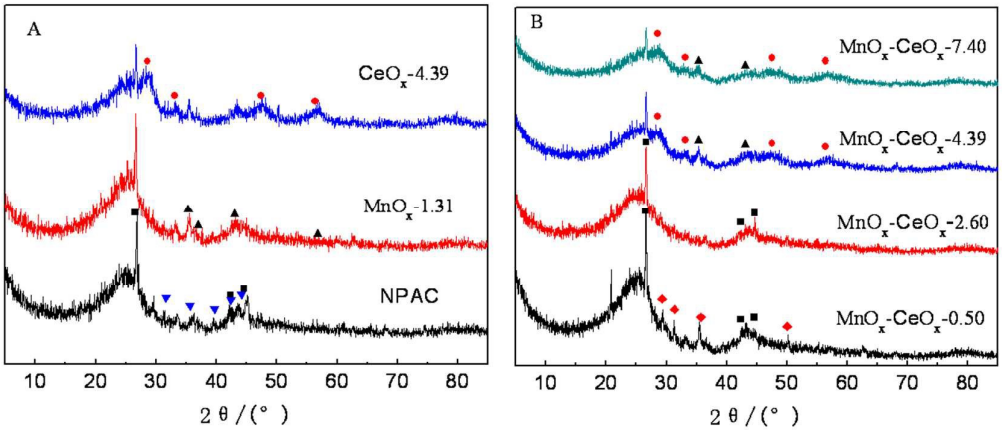

Fig. 2 XRD analysis of NPAC and modified activated coke(■:graphite;●: CeO_2;▼: Carbon;▲: Mn_3O_4;◆cerium manganese carbide.)

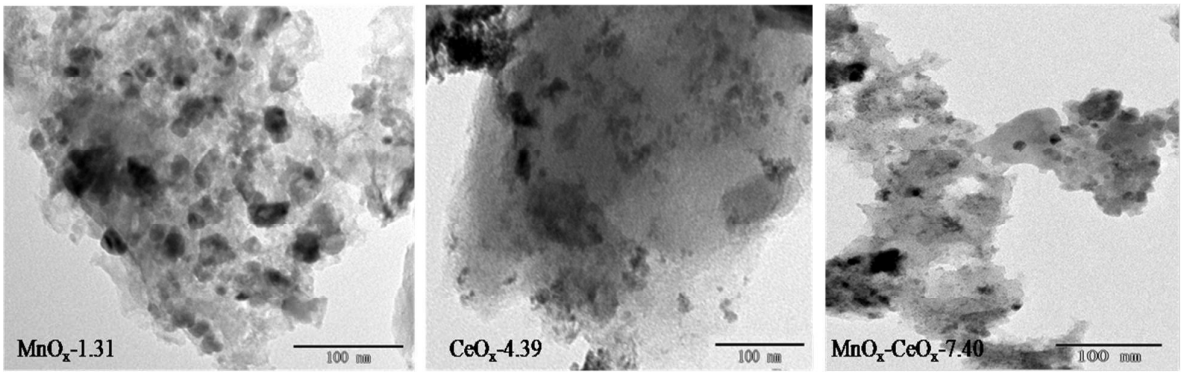

Fig. 3 TEM images of MnOx-1.31, CeOx-4.39 and MnOx-CeOx-7.40 samples.

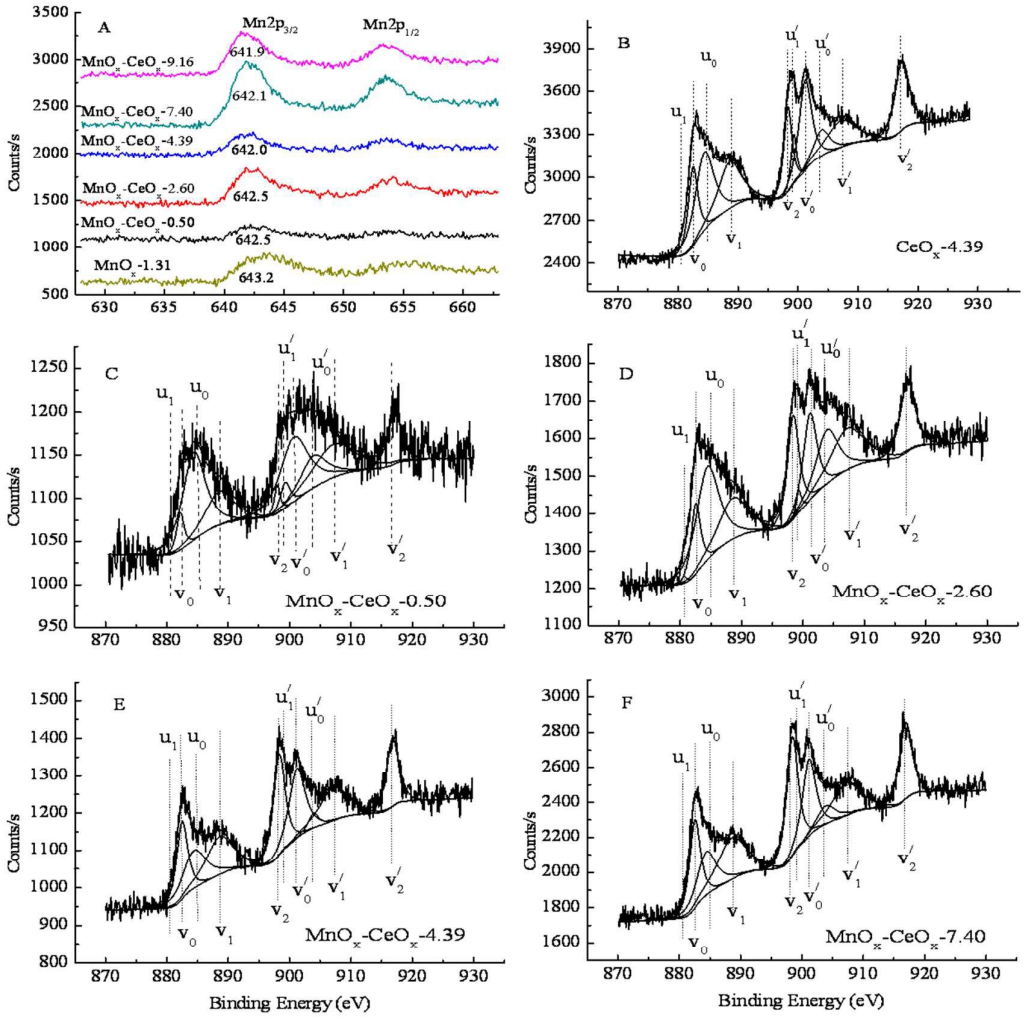

Fig. 4 Mn_{2p} and Ce_{3d} XPS spectra for the modified activated coke.

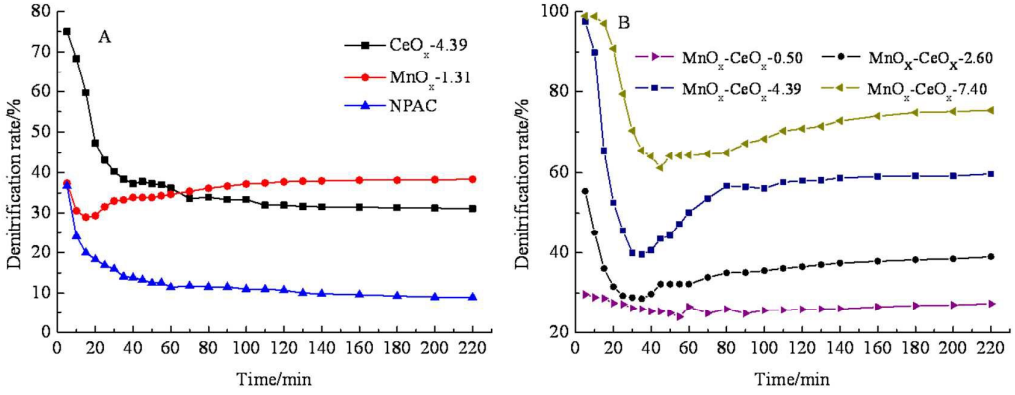

Fig. 5 Denitrification performance of NPAC and modified activated coke samples.

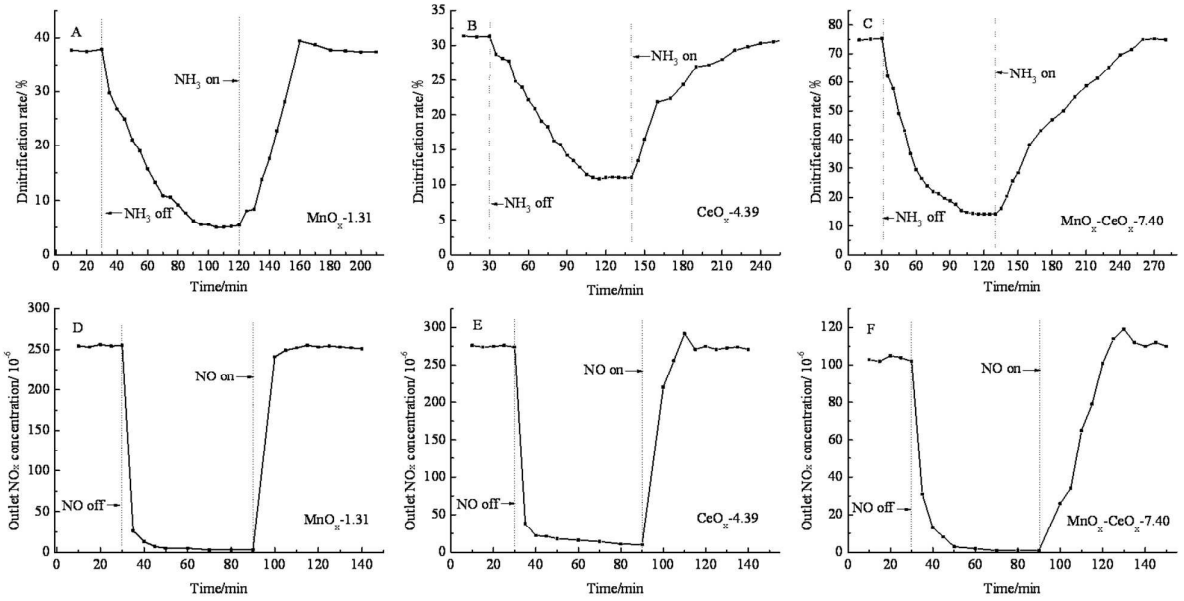

Fig. 6 Transient response experiment of NH_3 and NO.

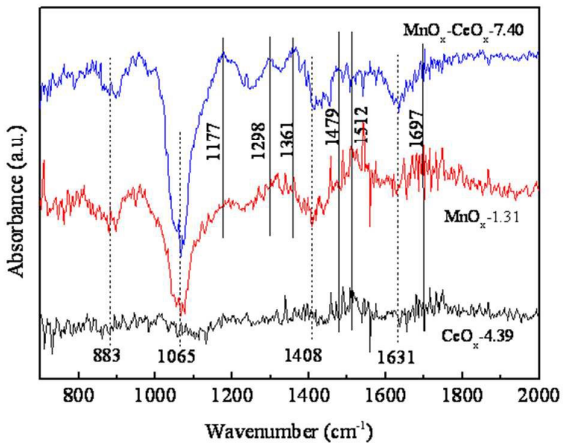

Fig. 7 Adsorption of NH_3 for 20min on the modified activated cokes at 140°C.

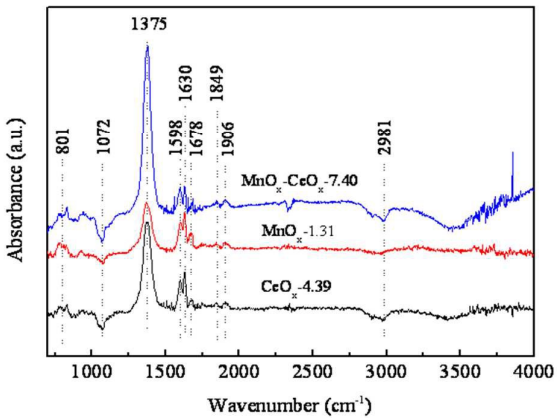

Fig. 8 Adsorption of NO for 20min on the modified activated cokes at 140°C.